PAPER • OPEN ACCESS

Vat polymerization 3D printing of composite acrylate photopolymer-based coated glass beads

To cite this article: Amirhossein Enayati Gerdroodbar *et al* 2023 *Mater. Res. Express* **10** 085306

Materials Research Express

PAPER

Vat polymerization 3D printing of composite acrylate photopolymer-based coated glass beads

Amirhossein Enayati Gerdroodbar[1,2], **Hura Alihemmati**[1,2], **Mohsen Zeighami**[1,2], **Mahdi Bodaghi**[3], **Abbas Z Kouzani**[4], **Behzad Pourabbas**[1,2,*] **and Ali Zolfagharian**[4,*]

[1] Faculty of Polymer Engineering, Sahand University of Technology, PO Box 51335-1996, Tabriz, Iran
[2] Nanostructured Materials Research Center, Department of Polymer Engineering, Sahand University of Technology, 5331817634, Tabriz, Iran
[3] Department of Engineering, School of Science and Technology, Nottingham Trent University, Nottingham NG11 8NS, United Kingdom
[4] School of Engineering, Deakin University, Geelong, Victoria 3216, Australia
[*] Authors to whom any correspondence should be addressed.

E-mail: pourabas@sut.ac.ir **and** a.zolfagharian@deakin.edu.au

Keywords: coated glass beads, digital light processing, 3D printing, mechanical properties

Supplementary material for this article is available online

OPEN ACCESS

RECEIVED
16 May 2023

REVISED
1 August 2023

ACCEPTED FOR PUBLICATION
18 August 2023

PUBLISHED
29 August 2023

Abstract

Vat photopolymerization-based three-dimensional (3D) printing techniques have been used as an efficient method for complex and special geometries in various applications. Composites are also a group of polymer materials that are obtained by adding a reinforcing component such as filler, fibres with different origins. Therefore, the development of 3D printable composites is paramount due to their high precision and speed of production. Glass beads (GBs) have been favorites as economical reinforcement agents for their chemical stability, water resistance in acidic environments, dimensional stability, and eco-friendly properties. In this study, 3D printable composites based on coated glass beads (CGBs) have been prepared. First, the beads are coated with ultraviolet (UV) curable resins to improve the interface with the polymer matrix. Then, CGBs are mixed with 3D printing resin and formulated for digital light processing (DLP) printing. The coating process is checked by scanning electron microscopy (SEM), and the mechanical properties of the 3D-printed composite structures have been evaluated by bending and compression tests. Also, the fracture behavior of cured resin has been checked with SEM. Mechanical property investigations have shown the success of the 3D printing of the CGBs into a photopolymer resin (PR) composite with behavior modification and compatibility of the interface with the matrix in practice.

Abbreviations

3D	Three-dimensional printing
AUVR	Acrylate UV curable resin
BG	Bioactive glass
CAD	Computer-aided design
CGBs	Coated glass beads
DLP	Digital light processing
FDM	Fused deposition modeling
GBs	Glass beads
HT-LS	High temperature laser sintering
PEK	Polyetherketone

PLLA/HGBs	Poly(L-lactide)/hollow GBs
PMMA	Poly(methyl methacrylate)
PR	Photopolymer resin
SEM	Scanning electron microscopy
SLA	Stereolithography
SLS	Selective laser sintering
SMPs	Shape memory polymers
VPP	Vat photopolymerization

1. Introduction

Three-dimensional (3D) printing involves adding layers of material to a 3D physical part based on designed 3D data with computer-aided design (CAD) software. Therefore, this method can be considered additive or layered production. 3D printing itself includes several techniques that are divided on different bases, such as the type of input feed, printing method [1–3]. Today, light-sensitive resins mean photopolymers, and their application for 3D printing objects with complex geometries has received much attention, resulting in a huge category of research devoted to them [4–6]. Therefore, many studies are being focused on improving printing methods and developing printing materials via the synthesis of high-performance polymers and modification of photopolymer systems [7–9]. During the 1980s, 3D techniques were limited mainly to decorative objects; however, the accuracy, repeatability, and range of 3D printing gradually expanded to the production of advanced industrial objects [10–12].

It is worth mentioning that vat photopolymerization (VPP) is one of the most attractive methods among 3D printing techniques. In this technique, by using light radiation with different wavelengths, such as ultraviolet, polymer chains will be obtained, a polymer network will be formed, and the solidification of the liquid resin will be visible. Based on this mechanism, various techniques such as stereolithography (SLA) and digital light processing (DLP) have been developed that belong to this category. The advantages of this technique are high accuracy, high speed, variety in formulation design, variety of print geometry, light source intensity control, and variety in wavelength selection [13]. This method was initially introduced for printing pure resins, but with the passage of time, it has been improved for use in suspension materials, ceramics, and polymer composites [14–16]. With the increasing need for this technique, it has been noticed and used in a wide range of applications, from dental implants and bone scaffolds to smart biomaterials for soft robotics, smart wearables, and microfluidic devices [17]. In addition to these applications, the design of materials and related processes in medical applications has received much attention today [17–22]. Meanwhile, research is underway in the direction of developing polymer characteristics for mechanics and biocompatibility, with tuning of mechanical properties achieved by altering printing process parameters. 3D printing processes such as Fused deposition modeling (FDM), selective laser sintering (SLS), stereolithography (SLA), and digital light processing (DLP) have also provided this platform for custom design. Safety gear, dental implants, and drug delivery systems are some of the additional medical applications that have been examined. The results point to the need for enhanced design methodologies to navigate the complicated choice space made possible by 3D printing [23–25]. In addition, for the improvement and development of vat photopolymerization-based techniques, the development of photopolymers and related materials such as photoinitiators, UV curing monomers and oligomers, and multi-functional cross-linkers is needed, and interesting works have been done in this regard recently. Meanwhile, the synthesis of new monomers and oligomers has a special place, and much research has been focused on these matters. The functional groups present on these monomers and oligomers can determine the type of photopolymerization mechanism, the speed of the 3D printing process, and the properties of the final part [26]. Based on the type of functional group available, free radical or ionic photopolymerization can be created, or based on monomers, simultaneous free radical and ionic photopolymerization can be activated [27–29]. Therefore, based on the type of monomer, the type of photoinitiator, the mechanism of photopolymerization will be determined [30, 31].

Acrylate [32, 33], methacrylate [32, 33], epoxy [34–36] and thiol [37, 38] monomers are of great importance in UV curing 3D printing methods. Alessandro *et al* later used vegetable oils as starting monomers and then acrylated them as photocuring agents in the presence of a photoinitiator [39]. Furthermore, Mahmoodian *et al* prepared nanocomposites with a low amount of filler based on acrylate monomers and investigated the mechanical properties of cured polymer [40]. Habib and colleagues also prepared the oligomer of epoxidized and acrylated soybean oils and obtained a UV-baking system along with other acrylate monomers [41]. Theoretically, one mole of hydrogen peroxide can epoxidize one molecule of the double bond in the oil. In

addition, Kulkarni *et al* synthesized UV-sensitive acrylate monomers and investigated their properties [42] while Li and colleagues synthesized UV-based urethane acrylate monomers, which used castor oil and pentaerythritol triacrylate acrylate monomer [43].

Polymeric materials are on track for improvement, for example, in the form of composite materials due to their reinforced properties [44–46]. Desired mechanical properties are among the significant parameters of the printed samples that are anticipated from the composite 3D printing resins, for which there has also been some interesting research [47, 48].

GBs have been favorites as an economical reinforcement agent for their chemical stability, water resistance in acidic environments, dimensional stability, and eco-friendly properties. The point here is that among all the available techniques for 3D printing, methods such as SLS and FDM, are suitable and effective for composites containing glass fillers. But along with all the advantages, they suffer from disadvantages such as low speed, low accuracy, and process limitations that cause a lack of progress and close competition with other techniques based on UV and polymer resins such as DLP and SLA. In this case, Zaki and colleagues used an extrusion-based 3D-printing approach, deploying the FDM process to print transparent phosphate glasses. Finally, parts with complex geometry have used this system in optical parts [49]. Das *et al* investigated the process and mechanical properties of glass bead particulate-filled functionally graded Nylon-11 composites produced by SLS. The results of the mechanical test showed that the tensile and compressive moduli increased with the increase of GBs volume fraction, and the strain at the breaking point and bending decreased [50]. Also, Chung *et al* studied the thermal expansion behavior and mechanical properties of GBs filled polyetherketone (PEEK) composite by high temperature laser sintering (HT-LS) [51]. Guo *et al* prepared polyamide/GBs composites made with multi-jet fusion technology. In this work, dimensional accuracy, surface roughness, surface hardness, mechanical stability, thermal stability, and flammability were studied and evaluated [52]. Mária Kováčová and colleagues prepared composites based on the biodegradable polymer polycaprolactone and hollow glass beads (GBs). This composite was prepared by the FDM method to produce filaments for use in 3D printing, and the main goal was to decrease the printing temperature below 100 °C using biodegradable polymers in combination with very cheap inert filler [53]. Following these cases, Cano *et al* studied the effect of temperature on the fracture behavior of polyamide 12 and glass-filled polyamide 12 processed by SLS [54]. In one of the latest studies, Gadelmoula *et al* investigated the tribological behavior of polyamide 12 composites filled with GBs by the SLS method [55].

Along with the investigations and studies done on the effect of GBs on the properties of polymer matrices, these particles have been considered for use in biological, pharmaceutical, and medical applications. In this regard, polymer composites containing these beads were also developed, so Shinzato *et al* investigated PMMA-based bioactive cement and the effect of GB filler content and histological change with time [56]. In continuation of this work, Shinzato *et al* studied the *in vivo* ageing test for a bioactive bone cement consisting of GB filler and PMMA matrix [57]. The use of these GBs is not limited to the mentioned cases, and the existing applications are also used as fillers for biocompatible and biodegradable polymer matrices. Hu *et al* investigated the morphology, crystalline behavior, and mechanical and thermal properties of poly(L-lactide)/hollow GBs (PLLA/HGBs) composite, which has been used as a substitute for petroleum plastics in recent years and is also popular in medicinal applications [58]. Yun *et al* prepared porous bioactive glass (BG) balls using a modified version of a polymer templating technique. These compounds derived from the sol–gel method have been introduced as suitable candidates for graft material for bone tissue regeneration due to their bioactivity and biodegradability. In general, the properties of these fillers were studied for their *in vitro* and *in vivo* biocompatibility [59].

Using higher loadings of the filler, or high-density stiff fillers, leads to undesirable properties of the 3D printing resins, such as high viscosity or instability of the fillers within the resin. The 3D printers based on SLS technology use powder materials for printing, resulting in high strength printed objects with limited resolution in addition to a relatively lower printing speed in comparison to DLP and SLA. Therefore, to print high strength objects while keeping resolution high, there is the possibility of using high strength fillers in the printing resin.

The present work is an attempt to combine SLS with DLP by using high-strength filler materials, and micron sized GBs in acrylate UV curable resin (AUVR) 3D printing to overcome the drawbacks of SLS and use the positive points of the DLP printing method. GBs have shown great chemical resistance, low moisture absorption, excellent mechanical strength, and appropriate dimensional stability. Therefore, in this work, the main goal is to directly modify and coat the GBs due to the applicability of the re-formulation of UV curable resin in DLP systems, which today have high accuracy and speed of production compared to other 3D printing methods. The purpose of the coating of GBs with PR has been to create a suitable interface with the polymer matrix in the printed piece because these glass particles do not have proper interaction or special functional groups, but at the same time, they can have excellent mechanical properties. This has been achieved by chemical surface modification and coating of micron-sized GBs to stabilize the beads in the resin body during printing.

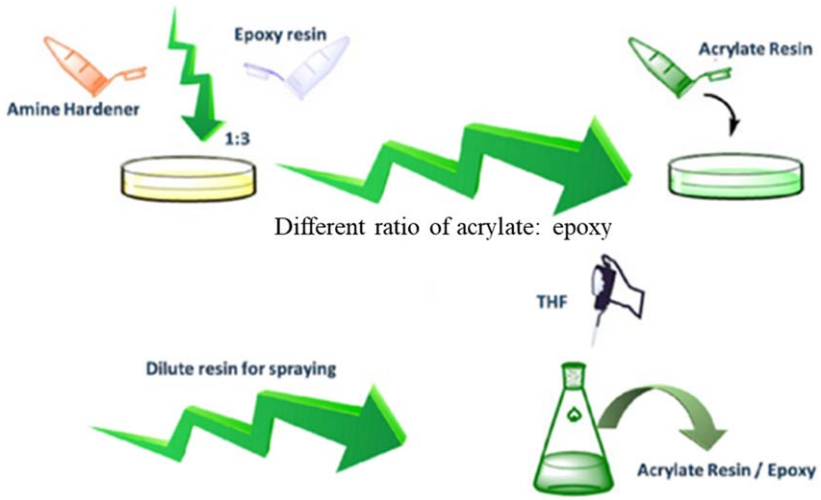

Figure 1. PR preparation process.

2. Materials and experiments

2.1. Materials preparations

AUVR (containing epoxy acrylate oligomer, 2-hydroxyethyl methacrylate monomer, multifunctional acrylate crosslinker, and photoinitiator) was kindly supplied by BasPar Technology Co., Iran, and GBs were obtained from Merck (2.5 g cm^{-3}, 40–250 μm). Other materials, including Cloisite 10 A (1.19 g cm^{-3}, powder), and Cloisite 30B (1.98 g cm^{-3}, powder), were purchased from Southern Clay, America. Montmorillonite K10 (1.9 g/cm^3, powder) was obtained from Fluka, Switzerland. Epoxy resin (1.12 g cm^{-3}, colorless liquid) with amine hardener from Parla-Iran, tetrahydrofuran (THF) (0.88 g cm^{-3}, colorless liquid), sulfuric acid (1.8 g cm^{-3}), and hydrogen peroxide (1.13 g cm^{-3}) were purchased from Merck.

2.2. Preparation of the AUVR and epoxy mixture: (PR)

The main purpose of this project related to the GBs surface coating with acrylate UV curable 3D printing resin. Epoxy resin has also been used for better adhesion and mechanical reinforcement of coatings. Therefore, according to figure 1, for an optimal formulation, a mixture of two resins in different ratios of 10% to 90% (w/w) has been prepared with various hardener contents. The results show that the weight ratio of 30:70 of acrylate/epoxy was appropriate, as shown in figure 1. Higher percentages of epoxy caused the beads to stick, and in higher proportions of acrylate resin, we couldn't observe a proper coating.

2.3. GBs sizing

In order to achieve a uniform size distribution of GBs, industrial standard sieves in the sizes of 53 μm (mesh 270) to 212 μm (mesh 70) were used, and the granulation method was such that the sieves were placed from top to bottom. The bottom was stacked in large to small sizes and the particles were granulated through mechanical vibration introduced by the machine for 15 min to make the particle size distribution uniform.

2.4. Surface cleaning and coating of GBs

Initially, Piranha solution (1:3 v/v sulfuric acid to hydrogen peroxide) was used to clean the beads' surfaces and remove all contamination. In the meantime, due to surface modification power of the Piranha solution and surface oxidation to increase the density of polar groups, the beads are ready for further modification. Therefore, 2 g of GBs were mixed for 15 min with the piranha and then washed with distilled water and used after drying at 100 °C. The modification process that was applied to the GBs rotary vessel is shown in figure 2. Heating was applied by an infrared lamp for preheating of the glass surface for 15 min A ratio of 1/10 (w/w) of beads/resin mixture was prepared, so GBs were transferred to the rotary vessel rotating at 50 RPM. For more precision in creating a uniform coating, PR was sprayed on GBs time to time and heated.

2.5. Preparation of AUVR filled with CGBs

CGBs have been added to AUVR in a different ratio and dispersed inside the matrix using an ultrasonic probe. After dispersion due to the different densities of the resin and the CGBs, precipitation was observed. Increasing the viscosity of the mixture could overcome the precipitation problem, which was achieved by using viscosity

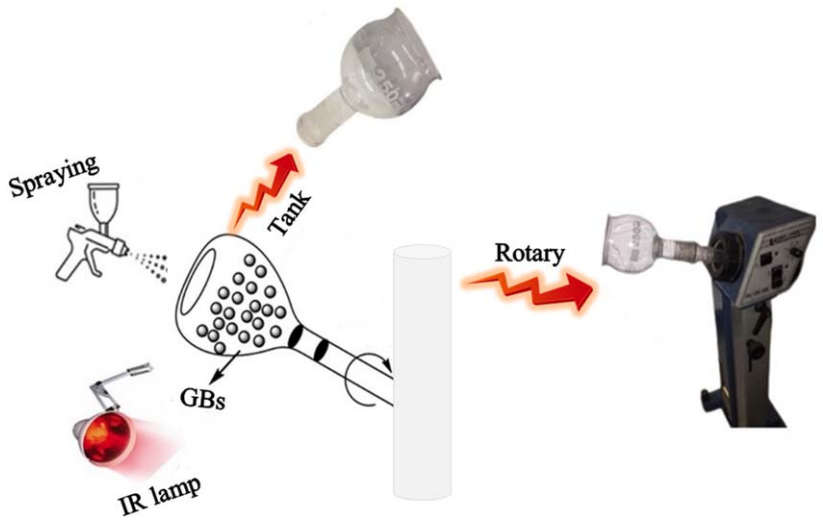

Figure 2. GBs coating method.

Table 1. Specifications of the prepared samples.

Code	Matrix	Modified filler	Filler percentage (wt.%)	Viscosity modifier Filler	Viscosity modifier Filler percentage (wt%)
R1	AUVR	—	—	—	—
R2	AUVR	CGBs	10	Cloisite 10 A	5
R3	AUVR	CGBs	20	Cloisite 10 A	5

modifier fillers. Therefore, three types of nanoparticles were examined, including cloisite 10 A, cloisite 30B, and montmorillonite K10 in the range of 1 to 5 wt%. The types of prepared formulations are also reported in table 1.

3. Characterizations

3.1. Conditions for 3D printing

A Prodent HD DLP printer made by Bonyan Mechatronics Co, Iran, was used for printing 3D samples. The printer had an LED projector ($\lambda = 405$ nm, 5w) and a printing volume of $64 \times 40 \times 134$ mm^3. Before printing, desired models were created using CATIA software, converted to STL and transferred to the printer as sliced image files. 3D printing was performed according to the predefined printing program at room temperature. After printing, samples were immersed in ethanol for 10 min to remove any uncured remaining resin. The samples were irradiated with ultraviolet light for post-curing.

3.2. Bending properties

To evaluate the mechanical properties of resin prepared with modified GBs, a three-point flexural test was used. Tests were performed according to the ASTM D790 standard at room temperature with a crosshead speed of 5 mm min^{-1} [60].

3.3. Compression mechanical properties

A uniaxial compression test was performed on a Z010 device according to the ASTM D695 standard test method at room temperature with a 5 mm min^{-1} test speed [60].

3.4. Microstructure and morphological observations

For morphological evaluation, a scanning electron microscope (SEM) was used to examine CGBs compatibility and fracture behavior of the 3D printed samples.

Figure 3. Images of 3D printed model samples.

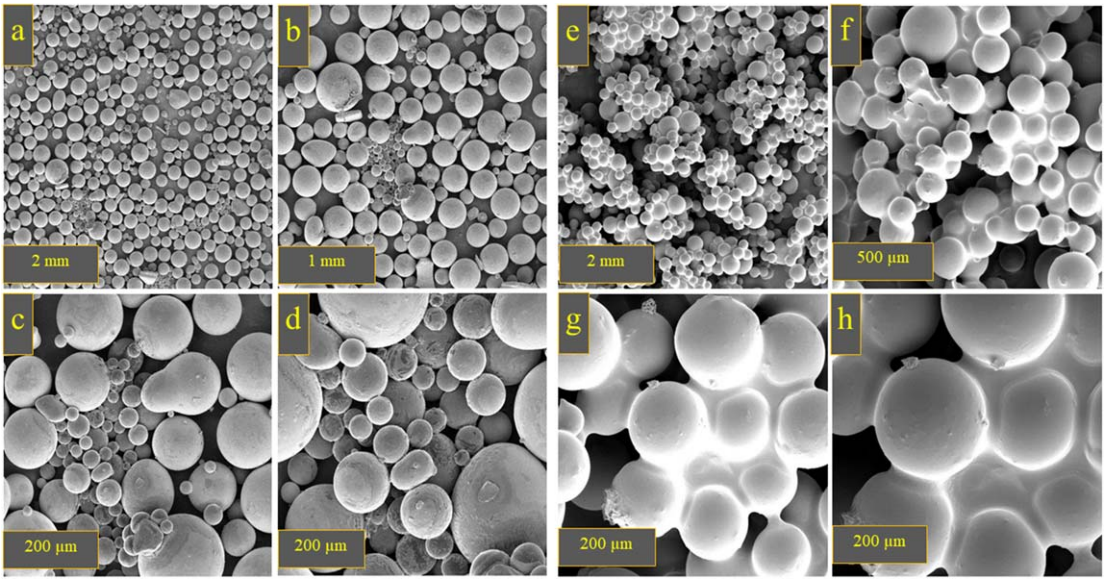

Figure 4. SEM result of GBs before coating at different magnifications of (a) 50, (b) 100, (c) 250, (d) 500 times, SEM images of CGBs with magnifications of (e) 50, (f) 150, (g) 350 and (h) 500 times.

4. Results and discussions

4.1. Printed sample

Samples with different geometries were printed using a DLP 3D printer. Figure 3 shows printed samples with prepared resins filled with modified GBs.

4.2. Surfaces characteristics of CGBs

Figures 4(a)–(d) show the SEM images of the GBs before and after coating. According to the images, the geometry of GBs is mostly spherical, which is important for surface coating and the final properties of the 3D-printed samples. After size sorting of the GBs, they were coated with UV-curable resins by spray coating. SEM images show the effect of modification and coating on the desired surface morphology.

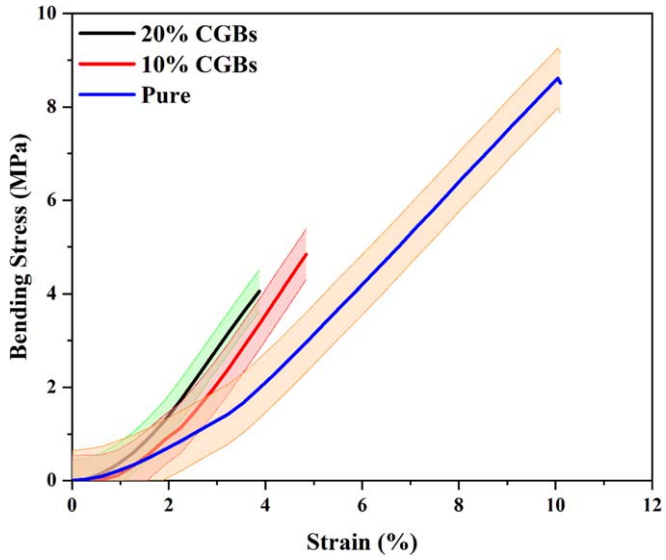

Figure 5. The stress–strain curves obtained from the bending tests for: Pure resin, 10 wt% CGBS, and 20 wt% CGBS.

Table 2. Bending results for CGBs filled AUVR compared to pure AUVR.

Sample	Bending modulus (MPa)	Ultimate strength (MPa)	Elongation at break (%)
Pure resin	86.56 ± 6.93	8.17 ± 0.54	8.70 ± 1.31
CGBS 10 wt%	94.98 ± 0.43	4.92 ± 0.64	5.00 ± 0.80
CGBS 20 wt%	136.72 ± 26.49	3.98 ± 0.44	3.11 ± 0.81

4.3. Mechanical properties of the printed samples

4.3.1. Bending test

To evaluate the mechanical properties, the bending mode according to ASTM D790 standard and compression test according to ASTM D695 standard were performed. The results of the bending test, including bending modulus, final strength, and strain at break, are given in table 2. Stress–strain diagrams for pure resin, samples with 10 wt% and 20 wt% CGBs are shown in figure 5. In the bending test, failure was observed to occur by cracking from the side of the specimen under stress. Resins filled with CGBs showed different behavior from the matrix in the face of stress and generally higher modulus compared to pure resin. Therefore, CGBS increases the modulus up to 60%. Increasing the modulus of the matrix due to GBs was observed to fulfill Kerner's equation (equation (1)). CGBs increase modulus with increasing volume percentage, completely in agreement with the experimental results from 86 MPa to 136 MPa for addition of 20 wt% CGBs. In equation (1), E_c: composite module, (Mpa) E_m: matrix module (Mpa), φ_f, φ_m: volume percentage of the matrix and filler, respectively; and υ_m: Poisson ratio of the matrix.

$$E_c = E_m\left(1 + \frac{15\varphi_f(1 + \upsilon_m)}{(8 - 10\upsilon_m)(1 - \varphi_m)}\right) \quad (1)$$

In contrast to bending modulus, CGBS has a weakening effect on bending strength, leading to decreased bending strength with increasing volume percentage of the CGBs. This can be attributed to their greater rigidity compared to the matrix, so that during stress loading, rigid particles prevent the deformation of the sample. As a result, strain at the break decreases, leading to decreased final strength. This behavior is compatible with the predictions of particle-filled systems provided by Piggot-Leinder (equation (2)). According to this equation, with increasing volume percentage of the filler, final strength decreases, as was confirmed by the experimental data. In equation (2), σ_c is composite stress, σ_m is matrix stress , λ is the stress concentration, x is the polymer-filler adhesion constant and, σ_f is filler stress.

$$\sigma_c = \lambda\sigma_m - x\sigma_f \quad (2)$$

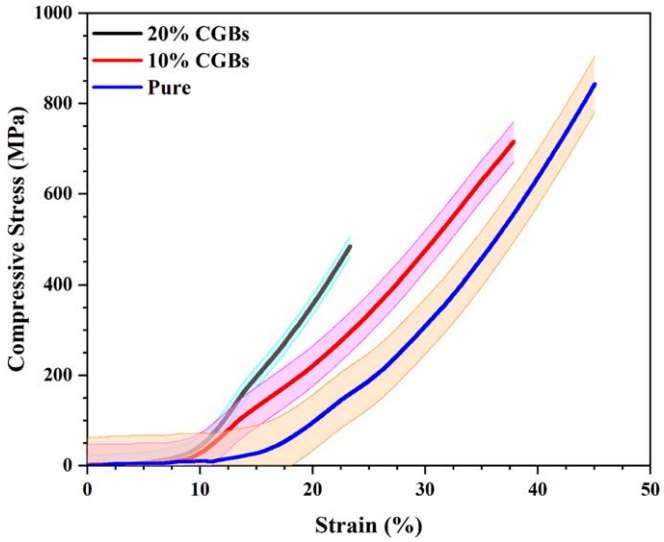

Figure 6. The stress–strain curve obtained from the compression test: (a): Pure resin, (b):10 wt% CGBs, (c):20 wt% CGBs.

Table 3. Compression results for results for CGBs filled AUVR compared to pure AUVR.

Sample	Ultimate strength (MPa)	Elongation at break (%)
Pure resin	827.87 ± 61.54	40.79 ± 0.54
CGBS 10 wt%	710.69 ± 44.43	34.85 ± 4.44
CGBS 20 wt%	473.59 ± 22.48	31.12 ± 1.45

4.3.2. Compression test

The results of the compressive tests are given in table 3. Stress–strain diagrams for pure specimens, 10 wt% and 20 wt% CGBS are shown in figure 6. It is observed that the results are consistent with the bending test. In both bending and compression tests, the presence of CGBs increases the modulus. On the other hand, CGBS decreases the ultimate strength and elongation by increasing the filler content. Also, strain at break shows that the CGBs reduce the toughness and strain at break of the samples from 8.70% for pure resin to 3.11% for resin includes 20 wt% CGBs. The correlation of the experimental results obtained from the bending and compression tests with the equations of Kerner and Piggot-Leinder indicates the effectiveness of the coating, the coating method, and the compatibility of CGBs with the acrylate-based matrix.

4.4. Microscopic examination and failure behavior of the 3D printed samples

Figure 7 shows the SEM images of the surface of the fractured specimens obtained after bending test. Samples containing CGBs show the effect of stress concentration over different parts of the sample which is related to the presence of CGBs. This is why pure resin shows a smooth surface after breaking. In general, CGBS, due to their higher inherent stiffness and rigidity, do not undergo deformation because of the applied force. In other words, they do not absorb energy during loading, and therefore, energy is absorbed mainly by the matrix, leading to fracture of the whole sample. According to SEM images in figure 7, CGBs have left holes on the surface after detachment from the matrix, with no trace of materials deflection or deformation around the holes, showing no energy concentration or energy dissipation around the particles.

Figure 8 shows the SEM images of the fracture surfaces of the specimens containing the CGBs filler and the cavities created on the surface of the specimens when the load is applied to them in the bending test. Figures 8(a) to 10(d) are related to samples containing 10 wt% CGBs with different magnifications, and figure 8(d) is related to samples containing 20 wt% CGBs. As can be seen in the SEM images, for the fracture surfaces of the samples containing 10 and 20 wt%, no deformation occurred during the application of load to the particles, and this caused a decrease in the final strength of the samples. In the SEM images of fracture surfaces of samples containing CGBs, holes were observed on the surface of the samples. The reason for the formation of these holes is that when the load is applied to the samples, the GBs tend to separate from the surface of the matrix. As a result,

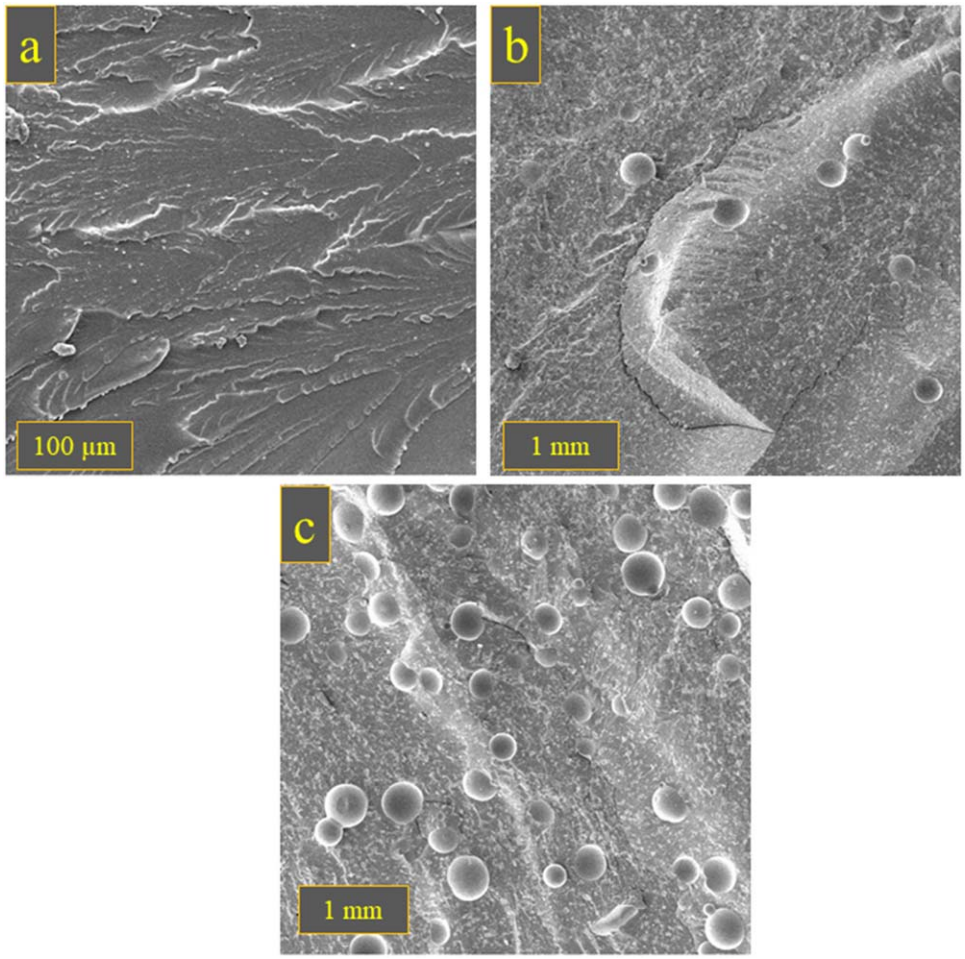

Figure 7. SEM images of fracture surface of specimens in the bending test: (a) Pure resin, (b) 10 wt% CGBs, (c) 20 wt% CGBs.

the volume fraction of the composite that carries the load collapses, and the sample matrix fills up and looks like a Swiss cheese.

Figure 9 shows that the interactions between the dispersed phase and the matrix are weakened by the greater content of the CGBs, which is related to the reduction of the distance between these particles. By increasing the content of CGBs to 20 wt%, we can see the reduction of the distance between the GBs, which is shown in figure 9 for 10 and 20 wt% CGBs in equal magnification. According to the pictures, it is possible to change the distance between the particles by changing the volume fraction of the CGBs.

4.5. Mathematical investigation of failure behavior

To investigate the failure behavior of samples, the Wu equation (equation (3)) has been used. This means that if the distance between the particles inside the matrix is greater than the critical value of the equation, the final behavior will be brittle; otherwise, the hardness of the material will increase.

$$ID_c = d\left[\left(\frac{K\pi}{6V_{fc}}\right)^{\frac{1}{3}} - 1\right] \tag{3}$$

Moreover, equation (3) shows the Wu equation. In this regard, V_{fc} is the critical fraction of particles, and for GBs, this fraction is equal to 12.5%. K is the equation constant and is equal to 1, and d is the average diameter of the particles scattered in the matrix, which is equal to 137 μm for the GBs. As a result, if the distance between the particles in the final sample matrix is greater than 83.84 μm, the sample behavior will be brittle. According to the SEM images shown in figure 10, the average distance between particles inside the matrix is greater than the critical value, so the behavior of the material will be brittle. The results obtained from the SEM images are consistent with the results obtained from the mechanical tests. According to the obtained results, the average distance between the CGBs inside the matrix at 10 wt% and 20 wt% is 460 μm and 240 μm, respectively. On the

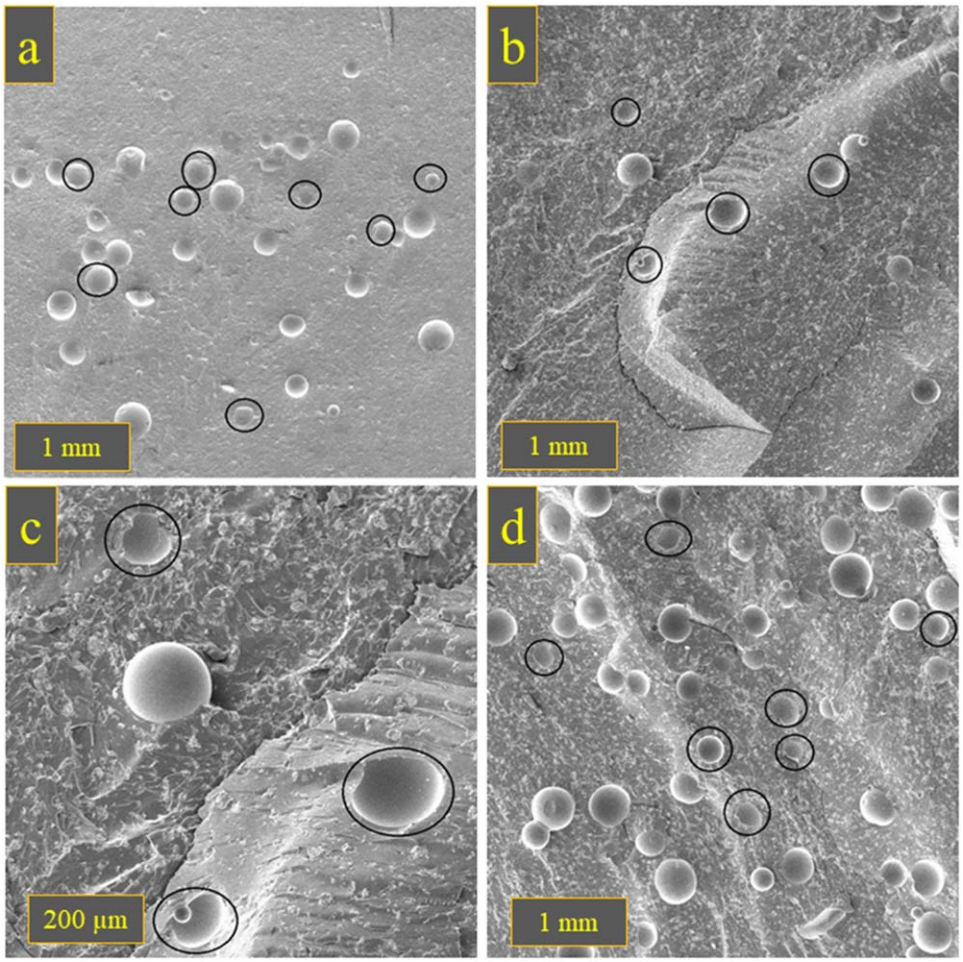

Figure 8. SEM images of fracture surfaces of specimens containing CGBs and cavities created on the specimen surface upon loading (a)–(c) 10 wt% (d) 20 wt%.

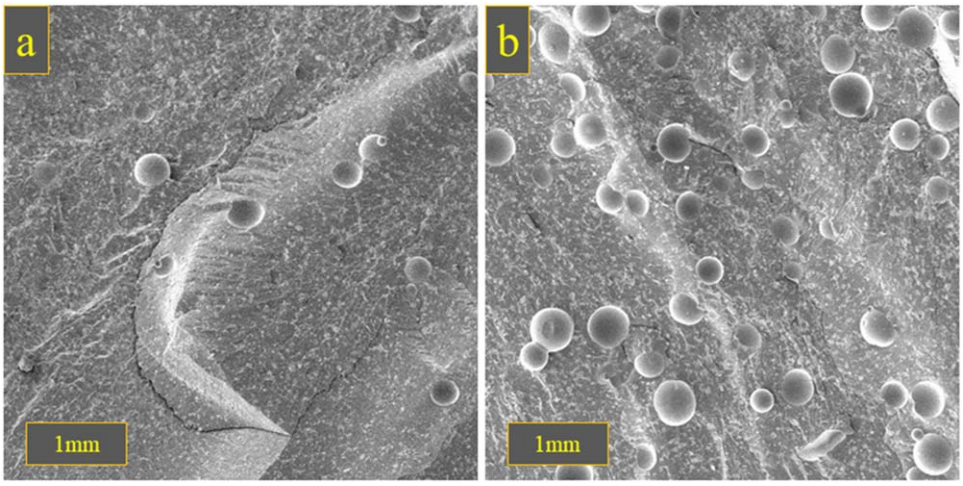

Figure 9. SEM images related to reducing particle spacing by increasing CGBs content (a) 10 wt% (b) 20 wt%.

other hand, it is possible that by increasing the weight percentage of CGBs to 30 wt%, the average distance between the particles will be less than the critical value of equation (3). However, according to the results, by increasing the weight percentage of GBs, the mechanical properties, such as final strength, are reduced due to separation of the beads and the increased hole content in the matrix.

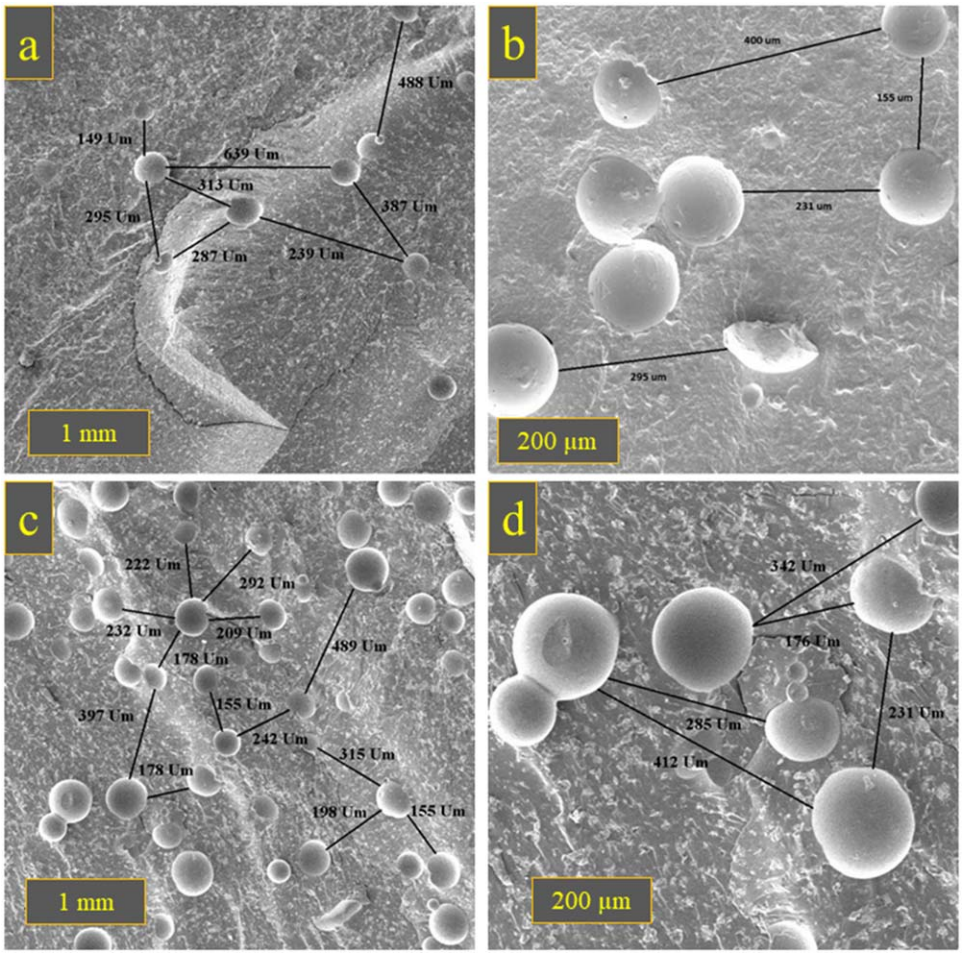

Figure 10. The distance between the CGBs inside the matrix: (a), (b) in 10 wt% and (c), (d) in 20 wt%.

5. Conclusion

In this paper, the effects of GBs' inclusion in acrylate-based photopolymer resin and its 3D printing are investigated. The effect of CGBs has been evaluated, and it has been found that mechanical properties such as ultimate flexural and compressive strengths, strain at fracture, bending modulus, and fracture behavior of specimens are strongly influenced by the addition of CGBs to acrylate-based photopolymer resin. The previously noted results are:

- Successful 3D printing showed that the prepared resins possessed the necessary rheological conditions to be used in 3D printers as well as printability of the filled resins.
- Bending and compression tests indicated that the GBs reduced the final bending and compressive strengths consistent with Piggot-Leinder's theory (by adding 20 wt% CGBs, the final strength decreased from 8.17 $\pm$ 0.54 MPa without CGBs to 3.98 $\pm$ 0.44 MPa in bending condition).
- The GBs reduce the strain at break in both flexural and compressive tests, proofing the brittle behavior of the fracture (by adding 20 wt% CGBs, the strain at break has decreased from 8.70 $\pm$ 1.31% without CGBs to 3.11 $\pm$ 0.87% in bending condition).
- Accordingly, compression and bending moduli were observed to be increased as a result of effect by CGBs, as predicated by Kerner's theory (by adding 20 wt% CGBs, the Modulus has increased from 86.56 $\pm$ 6.93 MPa without CGBs to 136.72 $\pm$ 26.49 MPa in bending condition).

These findings provide researchers with new directions for 3D printing the coated GBs into an acrylate-based photopolymer resin composite with behavior modification and compatibility at the interface with the matrix.

Data availability statement

All data that support the findings of this study are included within the article (and any supplementary files).

ORCID iDs

Amirhossein Enayati Gerdroodbar https://orcid.org/0000-0003-1834-1447
Hura Alihemmati https://orcid.org/0000-0001-7797-8865
Mahdi Bodaghi https://orcid.org/0000-0002-0707-944X
Ali Zolfagharian https://orcid.org/0000-0001-5302-360X

References

[1] Bozkurt Y and Karayel E 2021 3D printing technology; methods, biomedical applications, future opportunities and trends *Journal of Materials Research and Technology.* **14** 1430–50
[2] Arif Z U, Khalid M Y, Noroozi R, Hossain M, Tian H, Shi H, Tariq A, Ramakrishna S and Umer R 2023 Additive manufacturing of sustainable biomaterials for biomedical applications *Asian J. Pharm. Sci.* **18** 100812
[3] Tamay D G, Usal T D, Alagoz A S, Yucel D, Hasirci N and Hasirci V 2019 3D and 4D printing of polymers for tissue engineering applications *Front. Bioeng. Biotechnol.* **7** 164
[4] Layani M, Wang X and Magdassi S 2018 Novel materials for 3D printing by photopolymerization *Adv. Mater.* **30** 1706344
[5] Zhao B, Li J, Li Z, Lin X, Pan X, Zhang Z and Zhu J 2022 Photoinduced 3D printing through a combination of cationic and radical RAFT polymerization *Macromolecules* **55** 7181–92
[6] Wendel B, Rietzel D, Kühnlein F, Feulner R, Hülder G and Schmachtenberg E 2008 Additive processing of polymers *Macromol. Mater. Eng.* **293** 799–809
[7] Ligon S C, Liska R, Stampfl J, Gurr M and Mülhaupt R 2017 Polymers for 3D printing and customized additive manufacturing *Chem. Rev.* **117** 10212–90
[8] Alghamdi S S, John S, Roy N R and Dutta N K 2021 Additive manufacturing of polymer materials: progress, promise and challenges *Polymers.* **13** 753
[9] Voet S D V, Guit J and Loos K 2021 Sustainable photopolymers in 3D printing: a review on biobased, biodegradable, and recyclable alternatives *Macromol. Rapid Commun.* **42** 2000475
[10] Li J, Boyer C and Zhang X 2022 3D printing based on photopolymerization and photocatalysts: review and prospect *Macromol. Mater. Eng.* **307** 2200010
[11] Zhang J and Xiao P 2018 3D printing of photopolymers *Polym. Chem.* **9** 1530–40
[12] Melilli G, Carmagnola I and Tonda-Turo C 2020 DLP 3D printing meets lignocellulosic biopolymers: carboxymethyl cellulose inks for 3D biocompatible hydrogels *Polymers.* **12** 1655
[13] Pagac M, Hajnys J, Ma Q P, Jancar L, Jansa J, Stefek P and Mesicek J 2021 A review of vat photopolymerization technology: materials, applications, challenges, and future trends of 3d printing *Polymers.* **13** 598
[14] Pei E, Loh G H, Harrison D, Almeida H D A, Verona M D M and Paz R 2017 A study of 4D printing and functionally graded additive manufacturing *Assem. Autom.* **37** 147–53
[15] Rathee S, Srivastava M, Maheshwari S, Kundra T K and Siddiquee A N 2018 Friction based additive manufacturing technologies: principles for building in solid state, benefits *Limitations, and Applications* (Taylor & Francis: CRC Press) (https://doi.org/10.1201/9781351190879)
[16] Srivastava M, Rathee S, Maheshwari S, Siddiquee A N and Kundra T K 2019 A review on recent progress in solid state friction based metal additive manufacturing: friction stir additive techniques *Crit. Rev. Solid State Mater. Sci.* **44** 345–77
[17] Ge Q, Jian B and Li H 2022 Shaping soft materials via digital light processing-based 3D printing: a review *Forces in Mechanics.* **6** 100074
[18] Behl M and Lendlein A 2007 Shape-memory polymers *Mater. Today* **10** 20–8
[19] Noroozi R, Arif Z U, Taghvaei H, Khalid M Y, Sahbafar H, Hadi A, Sadeghianmaryan A and Chen X 2023 3D and 4D bioprinting technologies: a game changer for the biomedical sector? *Ann. Biomed. Eng.* **51** 1–30
[20] Sun J Y, Zhao X, Illeperuma W R, Chaudhuri O, Oh K H, Mooney D J, Vlassak J J and Suo Z 2012 Highly stretchable and tough hydrogels *Nature* **489** 133–6
[21] Dong Y, Wang S, Ke Y, Ding L, Zeng X, Magdassi S and Long Y 2020 4D printed hydrogels: fabrication, materials, and applications *Adv. Mater. Technol.* **5** 2000034
[22] Zhang Y F, Ng C J X, Chen Z, Zhang W, S.l Panjwani K, Kowsari H Y, Yang Q and Ge 2019 Miniature pneumatic actuators for soft robots by high-resolution multimaterial 3D printing *Adv. Mater. Technol.* **4** 1900427
[23] Arefin A M E, Khatri N R, Kulkarni N and Egan P F 2021 Polymer 3D printing review: materials, process, and design strategies for medical applications *Polymers.* **13** 1499
[24] Zeenat L, Zolfagharian A, Sriya Y, Sasikumar S, Bodaghi M and Pati F 2023 4D Printing for vascular tissue engineering: progress and challenges *Adv. Mater. Technol.* **202300200**
[25] Haleem A, Javaid M, Singh R P and Suman R 2021 Significant roles of 4D printing using smart materials in the field of manufacturing *Advanced Industrial and Engineering Polymer Research.* **4** 301–11
[26] Liang R, Gu Y, Wu Y, Bunpetch V and Zhang S 2020 Lithography-based 3D bioprinting and bioinks for bone repair and regeneration *ACS Biomaterials Science & Engineering.* **7** 806–16
[27] Chittavanich P, Miller K and Soucek M 2012 A photo-curing study of a pigmented UV-curable alkyd *Prog. Org. Coat.* **73** 392–400
[28] Xu W, Wang X, Sandler N, Willför S and Xu C 2018 Three-dimensional printing of wood-derived biopolymers: a review focused on biomedical applications *ACS Sustainable Chemistry & Engineering.* **6** 5663–80
[29] Patil D M, Phalak G A and Mhaske S 2017 Design and synthesis of bio-based UV curable PU acrylate resin from itaconic acid for coating applications *Des. Monomers Polym.* **20** 269–82
[30] Dai J, Ma S, Liu X, Han L, Wu Y, Dai X and Zhu J 2015 Synthesis of bio-based unsaturated polyester resins and their application in waterborne UV-curable coatings *Prog. Org. Coat.* **78** 49–54

[31] Voet V S, Strating T, Schnelting G H, Dijkstra P, Tietema M, Xu J, Woortman A J, Loos K, Jager J and Folkersma R 2018 Biobased acrylate photocurable resin formulation for stereolithography 3D printing *ACS omega.* **3** 1403–8
[32] Barkane A, Platnieks O, Jurinovs M and Gaidukovs S 2020 Thermal stability of UV-cured vegetable oil epoxidized acrylate-based polymer system for 3D printing application *Polym. Degrad. Stab.* **181** 109347
[33] Su Y, Lin H, Zhang S, Yang Z and Yuan T 2020 One-step synthesis of novel renewable vegetable oil-based acrylate prepolymers and their application in UV-curable coatings *Polymers.* **12** 1165
[34] Baroncini E A, Yadav S K, Palmese G R and Stanzione III J F 2016 Recent advances in bio-based epoxy resins and bio-based epoxy curing agents *J. Appl. Polym. Sci.* **44103** 133
[35] Sahoo S K, Khandelwal V and Manik G 2018 Development of toughened bio-based epoxy with epoxidized linseed oil as reactive diluent and cured with bio-renewable crosslinker *Polym. Adv. Technol.* **29** 565–74
[36] Vitale A, Sangermano M, Bongiovanni R, Burtscher P and Moszner N 2014 Visible light curable restorative composites for dental applications based on epoxy monomer *Materials.* **7** 554–62
[37] Lowe A B 2010 Thiol-ene 'click' reactions and recent applications in polymer and materials synthesis *Polym. Chem.* **1** 17–36
[38] Fu A, Gwon K, Kim M, Tae G and Kornfield J A 2015 Visible-light-initiated thiol–acrylate photopolymerization of heparin-based hydrogels *Biomacromolecules.* **16** 497–506
[39] Pelletier H, Belgacem N and Gandini A 2006 Acrylated vegetable oils as photocrosslinkable materials *J. Appl. Polym. Sci.* **99** 3218–21
[40] Mahmoodian M, Pourabbas B and Arya A B 2010 Preparation and characterization of Bis-GMA/TEGDMA/clay nanocomposites at low filler content regimes *J. Compos. Mater.* **44** 1379–95
[41] Habib F and Bajpai M 2011 Synthesis and characterization of acrylated epoxidized soybean oil for UV cured coatings *Chemistry & Chemical Technology* **5** 317–26
[42] Kulkarni R, Chaudhari M and Mishra S 2013 UV cure acrylate monomers: synthesis, analysis and storage *Pigment & Resin Technology* **42** 53–67
[43] Li K, Shen Y, Fei G, Wang H and Li J 2015 Preparation and properties of castor oil/pentaerythritol triacrylate-based UV curable waterborne polyurethane acrylate *Prog. Org. Coat.* **78** 146–54
[44] Vyas A, Garg V, Ghosh S B and Ghosh S B 2022 Photopolymerizable resin-based 3D printed biomedical composites: Factors affecting resin viscosity *Materialstoday: Proceedings* **62** 1435–9
[45] Guit J, Tavares M B L and Hul J J 2020 Photopolymer resins with biobased methacrylates based on soybean oil for stereolithography *ACS Applied Polymer Materials.* **2** 949–57
[46] Sideridis E and Papadopoulos G A 2004 Short-beam and three-point-bending tests for the study of shear and flexural properties in unidirectional-fiber-reinforced epoxy composites *J. Appl. Polym. Sci.* **93** 63–74
[47] Piggott M R and Leidner J 1974 Misconceptions about filled polymers *J. Appl. Polym. Sci.* **18** 1619–23
[48] Wu S 1985 Phase structure and adhesion in polymer blends: a criterion for rubber toughening *Polymer* **26** 1855–63
[49] Zaki R M *et al* 2020 Direct 3D-printing of phosphate glass by fused deposition modeling *Mater. Des.* **194** 108957
[50] Chung H and Das S 2006 Processing and properties of glass bead particulate-filled functionally graded Nylon-11 composites produced by selective laser sintering *Materials Science and Engineering:* A **437** 226–34
[51] Wang Y, James E and Ghita O R 2015 Glass bead filled polyetherketone (PEK) composite by high temperature laser sintering (HT-LS) *Mater. Des.* **83** 545–51
[52] Guo B, Xu Z, Luo X and Bai J 2021 A detailed evaluation of surface, thermal, and flammable properties of polyamide 12/glass beads composites fabricated by multi jet fusion *Virtual and Physical Prototyping.* **16** S39–52
[53] Kováčová M, Vykydalová A and Špitálský Z 2023 Polycaprolactone with glass beads for 3D printing filaments *Processes.* **11** 395
[54] Cano A J, Salazar A and Rodríguez J 2018 Effect of temperature on the fracture behavior of polyamide 12 and glass-filled polyamide 12 processed by selective laser sintering *Eng. Fract. Mech.* **203** 66–80
[55] Gadelmoula A and Aldahash S A 2023 Tribological properties of glass bead-filled polyamide 12 composite manufactured by selective laser sintering *Polymers.* **15** 1268
[56] Shinzato S, Nakamura T, Kokubo T and Kitamura Y 2002 PMMA-based bioactive cement: Effect of glass bead filler content and histological change with time *Journal of Biomedical Materials Research: An Official Journal of The Society for Biomaterials, The Japanese Society for Biomaterials, and The Australian Society for Biomaterials and the Korean Society for Biomaterials* **59** 225–32
[57] Shinzato S, Nakamura T, Kawanabe K and Kokubo T 2004 *In vivo* aging test for a bioactive bone cement consisting of glass bead filler and PMMA matrix *Journal of Biomedical Materials Research Part B: Applied Biomaterials: An Official Journal of The Society for Biomaterials, The Japanese Society for Biomaterials, and The Australian Society for Biomaterials and the Korean Society for Biomaterials.* **68** 132–9
[58] Hu X, Xu H S and Li Z M 2007 Morphology and properties of poly (L-lactide) (PLLA) filled with hollow glass beads *Macromol. Mater. Eng.* **292** 646–54
[59] Yun H S, Park J W, Kim S H, Kim Y J and Jang J H 2011 Effect of the pore structure of bioactive glass balls on biocompatibility *in vitro* and *in vivo Acta Biomater.* **7** 2651–60
[60] Khalid M Y, Arif Z U, Sheikh M F and Nasir M A 2011 Mechanical characterization of glass and jute fiber-based hybrid composites fabricated through compression molding technique *Int. J. Mater. Form.* **14** 1085–95